Supplementary Information

Hybrid Dispersion Laser Scanner

K. Goda[1,2,3], A. Mahjoubfar[1,2], C. Wang[1], A. Fard[1,2], J. Adam[1], D. R. Gossett[2,3], A. Ayazi[1], E. Sollier[3], O. Malik[1], E. Chen[1], Y. Liu[1], R. Brown[1], N. Sarkhosh[1], D. Di Carlo[2,3] & B. Jalali[1,2,3,4]

[1]*Department of Electrical Engineering, University of California, Los Angeles, California 90095*

[2]*California NanoSystems Institute, Los Angeles, California 90095*

[3]*Depatment of Bioengineering, University of California, Los Angeles, California 90095*

[4]*Department of Surgery, David Geffen School of Medicine, University of California, Los Angeles, California 90095*

Axial resolution in surface vibrometry with HDLS. The axial resolution of the surface vibrometer with HDLS can be obtained from the normalized intensity of the interferometer outputs, which is given by

$$\xi = [1 \pm \cos 2k(z_0 + z)]/2 \,, \tag{11}$$

where k is the wavenumber, z_0 is the initial offset to the sample arm length with respect to the reference arm length, and z is the displacement caused by the vibrating target. Here the plus and minus signs in the equation correspond to the transmission and reflection of the input light. Also, we have assumed that the beamsplitter's split ratio is 50/50 and the reference mirror and sample are equally reflective to maximize the visibility of the normalized intensity. Differentiating Eq. (11) with respect to z yields

$$d\xi/dz = \mp k \sin 2k(z_0 + z) \,, \tag{12}$$

which can be used to obtain the minimum detectable depth change,

$$|dz| = 2^{-b}/k \sin 2k(z_0 + z) \,, \tag{13}$$

where b is the bit depth and $d\xi = 2^{-b}$ has been used. Our digitally improved ENOB is 8.3 bits whereas the ENOB is 5.5 bits, leading to a sub-nanometer axial resolution of 0.4 nm.

Inertial microfluidics. In finite-inertia confined channel flows the position of particles or cells in the directions perpendicular to primary channel flow can be altered by inertial lift forces as well as secondary flows induced by channel curvature. Both of these inertial effects have been manipulated to control the position of cells within microfluidic systems[33,40] for focusing for cytometry applications and cell or particle sorting. As a focusing mechanism inertial focusing is attractive as it does not require bulky reservoirs of sheath fluid or external forces. A simple design is used here to control cell position and velocity. From the perspective of the scanner, cells are positioned at the channel centerline. However, they may occupy two distinct distances from the scanner; particles in either position will travel downstream at the same velocity due to the symmetry of the parabolic velocity profile which is characteristic of pressure-driven microfluidic channels.

Microfluidic device fabrication. The inertial microfluidic device was fabricated in thermoset polyester (TPE) bonded to a beamsplitter. Our previously reported design[41] was fabricated using standard photolithographic methods and techniques reported by Kuo *et al*[42] and Fiorini *et al*[43]. PEEK (Polyetheretherketone) tubing was firmly sealed to the channel inlets and outlets to provide a strong interface for conducting fluid through the channel. For a more detailed protocol, see Sollier *et al*[44].

Digital signal and image processing for the HDLS-based flow cytometry experiment. As a first step, the 1D data sequence is chopped into frames whose frame length roughly corresponds to the laser repetition rate (90.8 MHz) divided by the digitizer's capture rate (50 GS/s). Consequently, each frame corresponds to one line recorded by the HDLS flow cytometer. As a second step, a correlation of a reference frame with all the following frames is performed. By a subsequently applied maximum search on each correlation frame, this correlation approach can be exploited in two different ways. First, the maximum values deliver a map of high signal-to-noise ratio (SNR) and low-SNR regions, which is used to distinguish image regions from neglected background regions. Second, the position of each correlation maximum determines each frame's walk-off with respect to the reference frame, which is subsequently used to synchronize the frames for image reconstruction.

The synchronized frames corresponding to the identified high-SNR regions are gathered to form a 2D matrix, where the first dimension corresponds to the scanned tines and the second dimension corresponds to the temporal evolution due to the microfluidic flow inside the channel. Due to the high frame rate of the HDLS flow cytometer, this second dimension provides a high grade of redundancy, depending on the actual flow speed of the system. By a temporal frame integration similar to the concept of the time-delay integration (TDI) technique for the readout of charge-coupled devices (CCDs)[45] , this redundancy is exploited for de-blurring and noise reduction.

Once the images are reconstructed, a median filter[45] is applied to slightly smoothen the image contours. In order to discriminate single cells from cell clusters, a watershed algorithm[47] is applied on the resulting image. Subsequently, the determined watershed regions measured and translated to the corresponding cell areas. In order to exclude cell clusters, which correspond to

false positive events in the resulting histogram, pictures with two or more adjacent watershed regions are consequently ignored.

Receiver operating characteristic (ROC) curve analysis. In order to generate an ROC curve, the scattering space has to be translated into a table of true positive rate (TPR) with respect to false positive rate (FPR). It is further required that at each FPR point, a discrimination threshold be used to yield the maximum TPR. This is crucial in order to obtain the maximum possible area under curve (AUC) from the ROC curve. For more information about the generation of an ROC curve, see Zweig and Campbell[48] and Pepe[49].

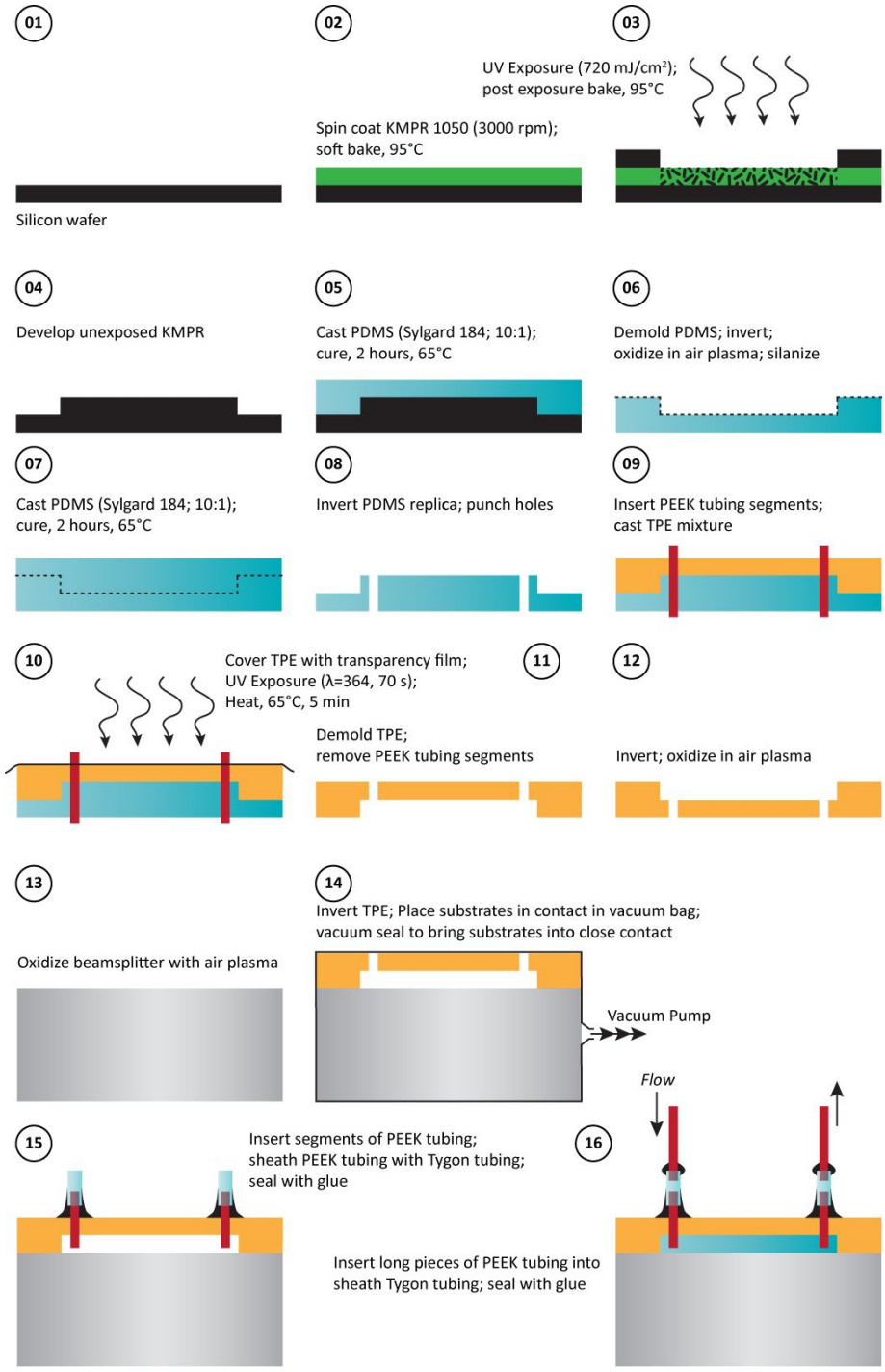

Supplementary Figure 1 | Procedure for the microfluidic device fabrication. Photolithography is used to fabricate a KMPR-on-silicon master mold (01-04). A PDMS replica is cured on the master mold and separated from the mold, and a new PDMS mold is then cured on the PDMS replica, resulting in the same polarity as the KMPR-on-silicon master (05-07).

Tubing inserts are created and TPE is semi-cured over the PDMS mold (08-10). The TPE replica is removed from the mold, bonded to the substrate, and finally cured (11-14). Tubings are inserted and secured with glue to allow high pressure injections (15-16).

Parameter	Value
Width of Microfluidic Channel at Interrogation Point	112 μm
Height of Microfluidic Channel at Interrogation Point	43 μm
Length of Microfluidic Channel	2.2 cm
Volumetric Flow Rate (Corresponding Mean Channel Velocity)	0.3 mL/min (1 m/s) 0.6 mL/min (2 m/s) 1.2 mL/min (4 m/s) 2.4 mL/min (8 m/s)
Channel Material	Thermoset Polyester
Maximum Pressure	≥150 psi (Limit of Pressure Sensor)
Young's Modulus	1.2 GPa
Light Transmittance	~90%
Swelling Ratio in Ethanol	1.0 (No Swelling)

Supplementary Table 1 | Specifications of the microfluidic device. To ensure stability in inertial focusing and ordering, the microchannel was fabricated by replica molding in thermoset polyester due to its ease of fabrication, high stiffness, ability to sustain high pressures, and resistance to ethanol which helps channel washing. Among these advantages, channel rigidity is especially critical to avoid undesirable fluid dynamic and optical effects which result if the channel deforms.

Supplementary Movie 1 | Nanomechanical surface vibration captured by the HDLS-based surface vibrometer. The diaphragm was driven to vibrate at 1 kHz. We monitored the vibration of the diaphragm surface with a sub-nanometer axial resolution of 0.4 nm at 100 kHz in real time. This is the first time that such a fast surface vibration was measured quantitatively in real time.

References

40. Di Carlo, D., Irimia, D., Tompkins, R. G. & Toner, M. Continuous inertial focusing, ordering, and separation of particles in microchannels. *Proceedings of the National Academic of Sciences of the Unites States of America* **104**, 18892-18897 (2007).
41. Gossett, D. R. & Di Carlo, D. Particle focusing mechanisms in curving confined flows. *Analytical Chemistry* **81**, 8459-8465 (2009).
42. Kuo, J. S., Ng, L., Yen, G. S., Lorenz, R. M., Schiro, P. G., Edgar, J. S., Zhao, Y., Lilm, D. S. W., Allen, P. B., Jeffries, G. D. M. & Chiu, D. T. A new USP Class VI-compliant substrate for manufacturing disposable microfluidic devices. *Lab on a Chip* **9**, 870-876 (2009).
43. Fiorini, G. S., Lorenz, R. M., Kuo, J. S. & Chiu, D. T. Rapid prototyping of thermoset polyester microfluidic devices. *Analytical Chemistry* **76**, 4697-4704 (2004).
44. Sollier, E., Murray, C., Maoddi, P. & Di Carlo, D. Rapid prototyping polymers for microfluidic devices and high pressure injections. *Lab on a Chip* **11**, 3752-3765 (2011).
45. McGraw, J. T., Angel, J. R. P. & Sargent, T. A. Applications of Digital Image Processing to Astronomy. *Proceedings of the Conference on Applications of Digital Image Processing to Astronomy, SPIE* (1980).
46. Lim, J. S. *Two-dimensional signal and image processing* (Prentice Hall, Englewood Cliffs, 1990).
47. Meyer, F. Topographic distance and watershed lines. *Signal Processing* **38**, 113-125 (1994).
48. Zweig, M. H. & Campbell, G. Receiver-operating characteristic (ROC) plots: a fundamental evaluation tool in clinical medicine. *Clinical Chemistry* **39**, 561-577 (1993).
49. Pepe, M. S. *The statistical evaluation of medical tests for classification and prediction* (Oxford University Press, New York, 2004).